IJMMM International Journal of Minerals, Metallurgy and Materials 矿物冶金与材料学报（英文版）

# Coordination states of metal ions in molten salts and their characterization methods

Xin Song, Shaolong Li, Shanshan Liu, Yong Fan, Jilin He, and Jianxun Song

Cite this article as:
Xin Song, Shaolong Li, Shanshan Liu, Yong Fan, Jilin He, and Jianxun Song, Coordination states of metal ions in molten salts and their characterization methods, *Int. J. Miner. Metall. Mater.*, 30(2023), No. 7, pp. 1261-1277. https://doi.org/10.1007/s12613-023-2608-7



---

*International Journal of Minerals, Metallurgy and Materials*
*Volume 30, Number 7, July 2023, Page 1261*
**https://doi.org/10.1007/s12613-023-2608-7**

**Invited Review**

# Coordination states of metal ions in molten salts and their characterization methods

*Xin Song*[1,2], *Shaolong Li*[1,2], *Shanshan Liu*[1,2], *Yong Fan*[3], *Jilin He*[1,2], *and Jianxun Song*[1,2]✉

1) School of Material Science and Engineering, Zhengzhou University, Zhengzhou 450001, China
2) Zhongyuan Critical Metals Laboratory, Zhengzhou University, Zhengzhou 450001, China
3) College of Resource and Environmental Engineering, Wuhan University of Science and Technology, Wuhan 430081, China
(Received: 4 November 2022; revised: 4 February 2023; accepted: 8 February 2023)

**Abstract:** The macroscopic characteristics of molten salts are governed by their microstructures. Research on the structures of molten salts provides the foundation for a full understanding of the physicochemical properties of molten salts as well as a deeper analysis of the microscopic electrolysis process in molten salts. Information about the microstructure of matter can be obtained with the help of several speculative and experimental procedures. In this review, the advantages and disadvantages of the various test procedures used to determine the microstructures of molten salts are compared. The typical coordination configurations of metal ions in molten salt systems are also summarized. Furthermore, the impact of temperature, anions, cations, and metal oxides ($O^{2-}$) on the structures of molten salts is discussed in detail. The accuracy and completeness of the information on molten salt structures need to be investigated by the integration of multiple methods and interdisciplinary fields. Information on the microstructure and coordination of molten salts deepens the understanding of the elementary elements of the microstructure of matter. This paper, which is based on the review of the coordination states of metal ions in molten salts, is hoped to inspire researchers to explore the inter-relationship between the microstructure and macroscopic properties of materials.

**Keywords:** coordination structure; characterization methods; molten salt composition; electrolysis

## 1. Introduction

The comprehension of matter and selected materials by researchers is based on the macroscopic physical characteristics of matter. The types of atoms and molecules present in a material and how these structures interact to form the microscopic structure, which in turn determines the macroscopic properties of the material. High-temperature molten salts are utilized frequently because of their high conductivity, wide electrochemical window, quick mass transfer, and other benefits [1]. They are used in a variety of fields, including electrochemical metallurgy, the recovery and utilization of secondary resources, functional materials, and the preparation of rechargeable batteries, wherein they can serve as an excellent medium for chemical reactions, energy transfer, and storage [2]. Numerous techniques for measuring the microstructures of molten salt, which can reflect the microstructures of substances from different angles, exist. The earliest investigation of the architecture of molten salts involved thermodynamic calculations [3]. The thermodynamic calculation method mainly uses calorimetry to determine the thermal properties of a molten salt system to obtain the structural information of the system indirectly. The theory of molten salt structure has been rapidly developed with the application of X-ray diffractometry [4], Raman spectroscopy [5], and nuclear magnetic resonance (NMR) [6]. Further research has been done on the microstructures and macroscopic thermodynamic characteristics of molten salts.

The study of the structures and characteristics of molten salts has been encouraged by the progressive advancement of spectroscopic technology and computer simulation technology and has led to a progression from a shallow to a profound understanding of molten salts. However, a comprehensive knowledge of the microstructures of molten salts has not yet been attained due to the intricacy of molten salts and the variable ion interactions in each molten salt. The findings of current studies remain limited, and considerable effort needs to be made to understand the structure of molten salts better. The test methods for obtaining the microstructures of molten salts and the comparison of their advantages and disadvantages are summarized in this paper. The typical coordination structures of metal ions in molten salt systems are also listed. In addition, research on the influencing factors of the structures of molten salts, such as temperature, anions, cations, and metal oxides ($O^{2-}$), will provide a reference for studies on the coordination structures of molten salts.

## 2. Characterization methods for molten salts

Given the particularity of the experimental conditions of

✉ Corresponding author: Jianxun Song E-mail: jianxun.song@zzu.edu.cn

high-temperature molten salts, the analytical methods used to study their structures are different from those used to analyze the structures of other substances at room temperature. The main methods are described below.

### 2.1. X-ray diffraction

The structure of molten salts can be analyzed and studied by using the excellent method of X-ray diffraction (XRD). When salts are melted, volume expansion exerts a diffusion effect on the XRD peaks of the original crystals. Consequently, the structural characteristics of the molten salt cannot be directly determined by XRD. The distribution function of the molten salt can be deduced by measuring the intensity of diffracted light.

Structural information, such as coordination numbers (CNs), average interatomic distances, average atomic displacements, and ordered domain sizes, can be derived from distribution functions. Thus, the microstructure of molten salts, the formation mechanism of ionic clusters in molten salts, and their evolution can be analyzed by means of high-temperature XRD.

Iwadate *et al.* [7] found that the CN of La–Cl was close to six when calculated by XRD and approximately seven when determined by X-ray absorption fine structure spectroscopy. These findings suggested that $La^{3+}$ is in an octahedral-like structure surrounded by 6 or 7 $Cl^-$.

High-temperature XRD can perform *in situ* measurement, and its temperature can also reach 1500°C or even 1600°C. However, the amount of information it obtains is limited. For molten disordered states, high-temperature XRD can yield the bond length, chemical bond, CN, and other information of the first nearest neighbor but cannot easily and effectively obtain the information of neighbors further away.

### 2.2. Raman spectroscopy

Raman spectroscopy can acquire the structural information of a substance by detecting the vibration and rotational energy levels of a molecule [5]. It is based on higher-order photon–molecule interactions and is considerably weaker than infrared absorption spectroscopy. It is suitable for the detection of symmetrical molecules without polarity.

Wang *et al.* [8] investigated the specifications of FLiNaK–$ScF_3$ and FLiNaK–$ScF_3$–$Li_2O$ melts at temperatures above 600°C by using Raman spectroscopy and also conducted density flooding theory (DFT) calculations. Dracopoulos *et al.* [9] studied a series of KF–$LnF_3$ (Ln = La, Ce, Nd, Sm, Dy, Yb) molten salt mixtures by utilizing Raman spectroscopy. Ma *et al.* [10] applied a combination of Raman spectroscopy and theoretical calculations to quantify the fluoride and fluorine oxide structures present in a $K_3AlF_6$–$Al_2O_3$ system and established a method for the quantitative analysis of molten salt structures by Raman spectroscopy.

In the analysis process, Raman spectroscopy has the advantages of simple operation, short determination time, and high sensitivity. However, it can only study the structural information of the corresponding group qualitatively, and the structural information of the corresponding group also needs further study on the basis of specific signals.

### 2.3. Neutron diffraction technique

The neutron diffraction technique (NDT) is a crystallographic method that is used to determine the atomic or magnetic structure of a material. This technique is similar to XRD, with the main difference being that the source of the radiation is different. The two techniques can complement each other. Given that neutrons are uncharged and have a strong penetration ability, samples can be determined in special containers. This approach is suitable for studying unusual samples, such as liquid, at high temperatures. Considering that different isotopes have different scattering lengths, an individual partial structure factor can be determined directly by isotope substitution [11].

Mitchell *et al.* [12] analyzed the ion pair distribution functions of RbCl molten salts by employing the NDT isotope substitution technique and found that Rb–Cl, Rb–Rb, and Cl–Cl had CNs of (6.9 ± 0.3), (13.0 ± 2.0), and (14.0 ± 2.0), respectively, and coordination distances of 3.18, 4.86, and 4.80 Å, respectively. Locke *et al.* [13] measured and reanalyzed the biased radial distribution functions of NaCl, RbCl, and CsCl molten salts by applying the isotope substitution method of neutron diffraction. They found that Na–Cl, Rb–Cl, and Cs–Cl had CNs of 4.83, 7.4, and 5.8, respectively, and ion spacings of 2.76, 3.2, and 3.4 Å, respectively.

NDT has numerous advantages, including sensitivity to light atoms, the ability to distinguish isotopes, the lack of radiation damage, and a penetration depth of several centimeters. Its main disadvantage is that its crystal cell parameters are inaccurate, and it is inconvenient to use because it requires a nuclear reactor.

### 2.4. NMR

NMR techniques have been proven to be a powerful tool for studying local structures around selected nuclei, cations, or anions. Its recent development for application at high temperatures has now enabled the study of mass melting systems and a more precise description of microstructures based on the properties of different species, average coordination, or first neighbors.

NMR measures [6] the frequency shift of the nucleus of an isotope due to different chemical environments, namely, the chemical shift $\delta$, which reflects the chemical information of the nucleus and its microscopic environment. It can be used to distinguish the microscopic structure of a substance.

Liu *et al.* [14] used $^{29}Si$ and $^{27}Al$ magnetic angle spinning NMR spectra to systematically study the thermal activation mechanism of silica alumina materials. Rollet *et al.* [15] investigated the local structures of molten $YF_3$–LiF and $LaF_3$–LiF binary systems by utilizing NMR technology. They also performed high-temperature NMR (HT NMR) experiments on a $LaF_3$–AF (A = Li, Na, K, Rb, Cs)–CaO mixture [16] to track the modification of the first rare earth coordination shell after oxide addition.

NMR technology has obvious advantages in resolving the microstructures of molten salts due to its high signal resolu-

tion and selective observation of characteristic elements. However, its weakness lies in its very poor sensitivity for structure capture when a sample is melted into the liquid state. Moreover, the rapid dynamic structure information of the liquid state is averaged such that the measured information is actually distorted and the information is inaccurate.

### 2.5. Extended X-ray absorption fine structure spectroscopy

Extended X-ray absorption fine structure spectra (EXAFS) can reflect structural information, including the near-neighboring atom centered on the absorption of the atom, which can be applied to the determination of amorphous structures [17]. The application of this technique to molten salt systems has been well studied by Okamoto *et al.* [18]. In addition to using the EXAFS technique directly to determine the microstructure of molten salts, Okamoto [19] also proposed calculating EXAFS spectra by extracting atomic snapshots obtained from molecular dynamics (MD) calculations, pointing out that this method is more rigorous and provides reliable structural information.

Through EXAFS, Okamoto *et al.* [20] calculated the CN of La–Cl to be (7.4 ± 0.5), which suggested the presence of $LaCl_6^{3+}$, $LaCl_7^{4-}$, or $LaCl_8^{5-}$ groups in the molten salt, with each unit group linked by a bridging Cl angle. Zissi *et al.* [21] deduced from Raman spectroscopy that La–Cl is a six-coordinated octahedral structure.

EXAFS has a high sensitivity to local atomic displacement, element characteristics, and vibration mechanics (accuracy above 0.01 Å). This technique is more suitable for *in situ* studies on structural transformations because it can be performed under a wide range of conditions. However, it is insensitive to stereoscopic structures.

### 2.6. Electrochemical analysis

The main electrochemical methods (EC) used in experimental procedures are cyclic voltammetry (CV), square wave voltammetry (SWV), chronopotentiometry (CP), and chronoamperometry (CA).

(1) CV is one of the most widely used electrochemical measurement methods [22]. The basic principle is to apply the triangular waveform pulse voltage to the closed loop formed by the working electrode and the opposite electrode, and change the potential on the working electrode/electrolyte interface at a certain rate. By forcing the active substance on the working electrode to undergo oxidation/reduction reaction, the response current of electrochemistry on the electrode can be obtained.

(2) SWV is a large-scale differential technique that superposes the symmetric square wave and the step voltage on the excitation signal of the working electrode [23]. It is a voltammetry method in which a rapid scanning step voltage is applied to the working electrode, and a small amplitude square wave is superimposed on each step to represent the potential–current relationship.

(3) CP is a transient measurement method employed to control the potential step size [24]. It controls the current flowing through the electrolytic cell and records the change in the potential with time to enable the study of the reaction mechanism.

(4) CA records the change in the current flowing through the system with time by controlling the potential of the electrolytic cell and obtains the current–time curve.

Zhu *et al.* [25] investigated the morphology and behavior of chromium ions in LiCl–KCl–$CrF_3$ and LiCl–KCl–LiF–$CrF_3$ melts by utilizing CV, SWV, chronopotentiometry, and Raman spectroscopy. Their results showed that the electrochemical reduction of Cr(III) into Cr(0) in LiCl–KCl–$CrF_3$ was a two-step process mediated by Cr(II) generation. In the molten salt medium, Cr(III) ions were present in the form of $CrCl_6^{3-}$, and $CrCl_{6-x}F_x^{3-}$ ($x \leq 3$) ions were less abundant. According to the CV results obtained at different potential scan rates, the diffusion coefficient of chromium ions in LiCl–KCl–$CrF_3$ was higher than that in LiCl–KCl–$CrCl_3$. Wu *et al.* [26] investigated the electrochemical reduction mechanism and electrocrystallization process of vanadium ions in the NaKClF system by applying CV, chronopotentiometry, and chronocurrent methods. Their results showed that the reduction reaction of $VO_3^-$ ions in the NaCl–KCl–NaF–$V_2O_5$ (abbreviated as NaKClF–$V_2O_5$) system was a reversible reaction involving five electrons in one step.

The advantages of the electrochemical method are its simplicity, high sensitivity, and good real-time performance. However, this method cannot directly detect the microstructure of molten salts and thus needs to be combined with other methods.

### 2.7. Computer simulation methods

The development of computer technology has enabled the simulation of microstructures on computers. The main computer simulation methods (Sim) are as follows [27].

(1) Quantum chemical (QC) essentially solves Schrödinger's equation and thus obtains the particle motion laws and parameters necessary to derive the other physical and chemical properties of molten salts [28]. QC makes direct use of fundamental principles and does not rely on empirical values, and it acquires very accurate results. Li *et al.* [29] studied the dynamic fluctuations of the $U^{3+}$ coordination structure in molten LiCl–KCl mixtures by using first-principles MD simulations. They calculated the radial distribution function and probability distribution of the CN. Their results revealed that the coordination structure of $U^{3+}$ in the molten mixture of LiCl–KCl–$UCl_3$ was dominated by a six-fold coordination structure.

(2) Monte Carlo (MC) is a statistical method that uses discrete random sampling [30]. It allows atoms to jump randomly in search of the lowest energy state to identify the properties of the material and to deduce the structure of the molten salt. The MC method is a random method, and its statistical results are ensemble-averaged. Baranyai *et al.* [31] calculated the structural parameters of a series of alkali metal chloride molten salts with MC simulation. They then analyzed the structural characteristics of alkali metal chlorides

by combining spectral diffraction techniques and the inverse MC method and found that the CNs of the molten salts LiCl, NaCl, and CsCl were 5.2, 4.85, and 6.1, respectively, which were then used as criteria.

(3) MD was developed on the basis of MC [32]. After the equation of motion is simulated, the time-dependent properties of the molten salt system can be obtained by solving this equation. However, no way to obtain the nuclear magnetic properties of the molten salt system exists. The MD method is a deterministic method whose statistical results are based on time averages. Bessada *et al.* [33–34] conducted a series of studies on the structures of metal fluorides, such as $ZrF_4$, $ThF_4$, and $LaF_3$, in metal fluorides and analyzed the experimental data with MD simulation calculations. He *et al.* [35] investigated the microstructure and dispersion behavior of LiF–$BeF_2$ molten salt by using Car–Parrinello MD simulations.

High-temperature molten salts have numerous microstructures. The microstructures of the material can be viewed from different angles and provide different information on the material. Fig. 1 shows the principles and available information on the characterization methods. All of these techniques enable the characterization of molten salt structures, though at various characteristic times and through differing processes. For example, XRD can only provide the total radial distribution function of a structure; Raman spectroscopy entails the vibration of a unit of known symmetry; NDT yields only the partial radial distribution function of a structure; NMR involves the modification of the magnetic field experienced by a specific nucleus as a result of its neighbors; EXAFS entails the diffraction of a photoelectron by nearby nuclei. These methods are thus complementary, and the local structure can be better described by comparing their results. In practical applications, multiple test sections can be used to verify and fill each other, and the microformation information of molten salt can be perfected on the whole surface. A comparison of the structural characterization methods is shown in Table 1.

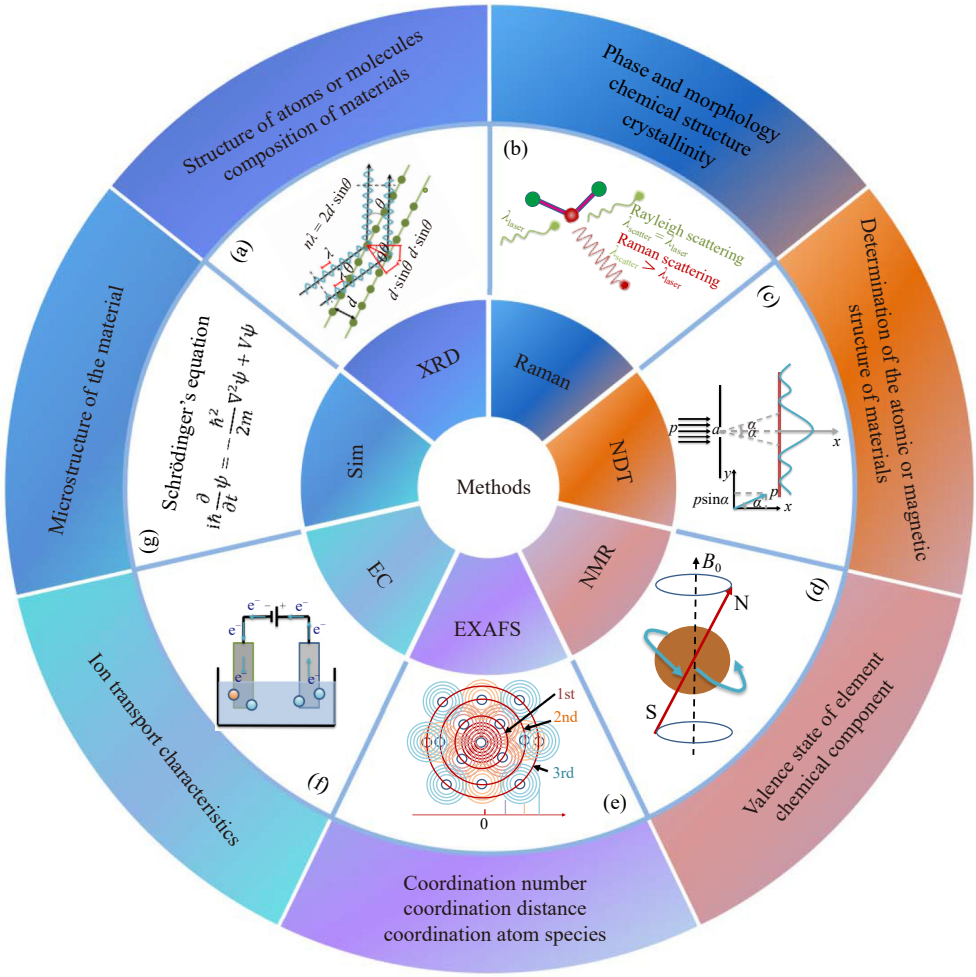


**Fig. 1. Principle and obtained information of characterization methods. In (a), $d$ is the crystal plane spacing, $\theta$ is the included angle between the incoming ray, the reflected ray and the reflected crystal plane, $\lambda$ is the wavelength, $n$ is the reflection order; in (b), $\lambda$ is the laser wavelength; in (c), $\alpha$ is the scattering angle, and $p$ is the scattering length; in (d), $B_0$ is the main magnetic field; in (e), the red circle is the coordination layer; in (g), $\Psi$ is the wave function of a physical system, i is the imaginary unit, $\hbar$ is reduced Planck's constant, $\partial/\partial t$ is partial differential for time, $m$ is the mass, $\nabla^2$ is the Laplace operator, and $V$ is the potential energy distribution in the system.**

**Table 1. Comparison of structural characterization methods**

| Method | Advantages | Disadvantages | Refs. |
|---|---|---|---|
| XRD | *In situ* measurement.<br>Reveals the formation mechanism and evolution of ion clusters. | The amount of information, such as valence and structure, obtained is relatively limited. | [4] |
| Raman | Does not need sample pretreatment.<br>Simple operation, short determination time, and high sensitivity. | Only the structural information of the corresponding group qualitatively. | [5] |
| NMR | High signal resolution.<br>Selective observation of characteristic elements. | The sensitivity to capture structure is very poorly measured, and information is actually distorted. | [6] |
| NDT | Sensitive to light atoms.<br>No radiation damage. | Inconvenient to use and inaccurate cell parameters.<br>Nuclear reactors are needed. | [11] |
| EXAFS | Highly sensitive to local atomic displacement, element characteristics, and vibration mechanics. | Insensitive to stereoscopic structures. | [17–19] |
| EC | Simple, sensitive, and real-time. | Cannot direct microstructures directly. | [22–24] |
| QC | Independent of empirical values and yields accurate results. | Limited to the simulation of smaller systems (less than 100 atoms) and has high computer requirements. | [28] |
| MC | Problems with statistical properties can be solved directly.<br>Does not need to discretize the problem of continuity. | Deterministic problems need to be transformed into stochastic problems.<br>More steps are usually required to calculate N. | [30] |
| MD | Physical quantities related to time can be used to calculate transport properties. | The nuclear magnetic properties of molten salt systems cannot be obtained. | [32] |

Note: Refs. represents references.

## 3. Structure of metal ions in molten salts

Molten salts are systems composed of ions, whether they are monomeric or pluralistic. The anions and cations in these systems are wrapped around each other and are randomly distributed. Common molten salts can be broadly classified into four categories: chloride salts, fluoride salts, nitrates, carbonates, and other molten salt systems. The typical coordination structures of metal ions in each molten salt system are discussed in the following sections.

### 3.1. Coordination structures of metal ions in molten chloride salts

The microstructures of molten chloride salts have become widely studied with the rapid development of high-temperature detection techniques, such as XRD, Raman spectroscopy, and computer simulation. This section briefly introduces the results of existing research on chloride molten salt systems.

Levy *et al.* [36] studied the structures of LiCl, KCl, and other chloride molten salts by using high-temperature liquid neutron diffraction and X-ray techniques and discovered that the ionic spacing of the high-temperature melt was smaller than that of the corresponding crystal at room temperature. They also found that the average CNs of ions were between 4 and 5 and that the ions were anisotropic within the first coordination layer. Førland *et al.* [37] studied the structural parameters of LiCl molten salts by applying MC computational simulation software and obtained a Li–Cl ionic spacing of 2.40 Å and CN of 4.3. Howe and McGreevy [38] investigated the microstructures of LiCl and NaCl molten salts by utilizing the isotope method and showed that Li–Cl in LiCl molten salts had an approximate tetrahedral structure. In addition, they calculated the CNs of Na–Na, Na–Cl, and Cl–Cl ion pairs to be (13.0 ± 0.5), 5.8, and (13.0 ± 0.5), respectively. Takag *et al.* [39] measured the radial distribution function of KCl molten salts via XRD and calculated the coordination distance and CN of K–Cl to be 3.05 Å and 4.1, respectively. Fig. 2 shows a snapshot of the chloride molten salt structure.

Jiang *et al.* [43] studied the structural properties of $CeCl_3$ in the LiCl–KCl–$CeCl_3$ system of chloride molten salts by applying MD computational simulation software and obtained the relationship among density, composition, and temperature. Kwon *et al.* [40] analyzed the basic mechanism of the spontaneous reduction of $Eu^{3+}$ into $Eu^{2+}$ in eutectic LiCl–KCl molten salt by first-principles calculation and characterized the main structural features of the solvated shell on the basis of the radial distribution function and CNs. Zhao *et al.* [41] investigated the local structure of LiCl–KCl and LiCl–KCl–$SmCl_3$ by using the radial distribution function, CN, and structure factor by performing QC simulation. They discovered that the average CNs of Li–Cl, K–Cl, and Cl–Cl pairs at 450°C were 4.33, 7.54, and 10.91, respectively. The first shell CN of Sm coordinated by Cl in LiCl–KCl–$SmCl_3$ melt was 6.56. In addition, $SmCl_3$ had little effect on the short-range order of the LiCl–KCl melt but affected the medium-range order distribution of the Li–Li melt. Akdeniz *et al.* [44–45] studied the ionic structures of $ThCl_4$, $ZrCl_4$, and $ThCl_4$–$ZrCl_4$ molten salts by using Raman scattering.

Okamoto *et al.* [46–47] studied the microstructure of $LaCl_3$ mixed with $LaCl_3$–ACl (A for alkali metal) molten salts in the molten state by using X-ray absorption fine structure ( XAFS) and MD and found that four ionic structures of $LaCl_6^{3-}$, $LaCl_7^{4-}$, $LaCl_8^{5-}$, and $LaCl_9^{6-}$ existed simultaneously in the $LaCl_3$ molten salt. They also mentioned that while the CN of the anion cluster decreased as the concentration of $La^{3+}$ in the molten salt decreased, the ionic clusters formed were all octahedral in structure. Song *et al.* [42] used QC simulations to study the structures and $UCl_3$ in the LiCl–KCl eutectic and calculated the corresponding CNs of Li–Cl, K–Cl, and Cl–Cl as 3.97–4.29, 6.69–7.32, and 9.99–11.39, respectively. In addition, in the molten mixture of LiCl–KCl–$UCl_3$, the positions of the first peaks of Li–Cl, K–Cl, and U–Cl were

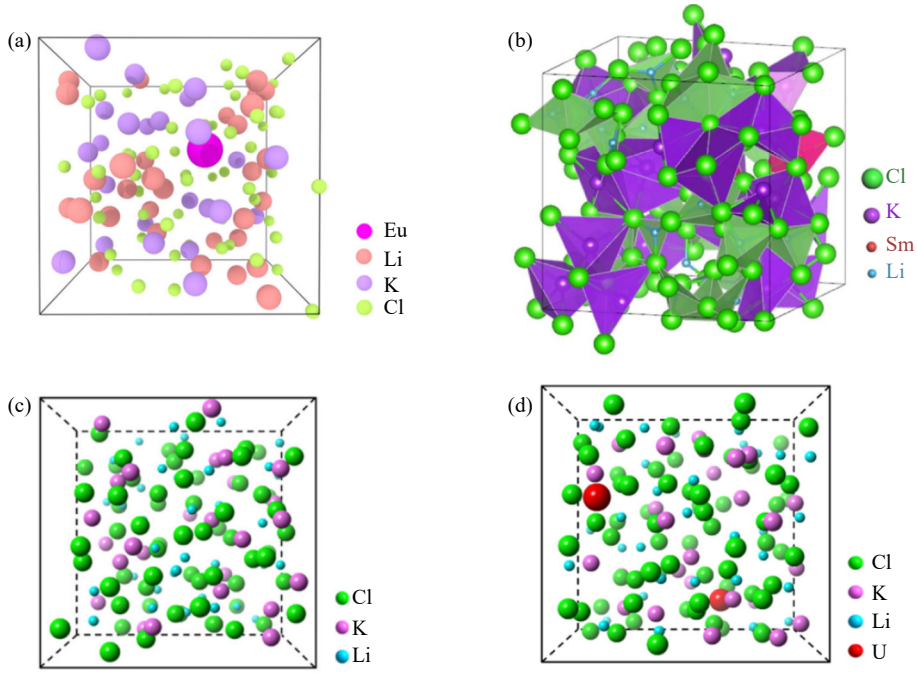


**Fig. 2. Snapshot of the chloride molten salt structure: (a) model system for Eu ions solvated in a LiCl–KCl eutectic molten salt [40]; (b) ion distribution in the LiCl–KCl–$SmCl_3$ system [41]; (c) ion distribution in the LiCl–KCl eutectic [42]; (d) ion distribution in molten LiCl–KCl–$UCl_3$ [42]. (a) C. Kwon, S.H. Noh, H. Chun, I.S. Hwang, and B. Ha, *Int. J. Energy Res.*, vol. 42, 2757-2765 (2018) [40]. Copyright John Wiley & Sons, Ltd. Reproduced with permission. (b) Reprinted from *J. Mol. Liq.*, 363, J. Zhao, Z.T. Liu, W.S. Liang, and G.M. Lu, Evaluation of the local structure and electrochemical behavior in the LiCl–KCl–$SmCl_3$ melt, art. No. 119818, Copyright 2022, with permission from Elsevier. (c, d) Reprinted from *J. Mol. Liq.*, 234, J. Song, S.P. Shi, X.J. Li, and L.M. Yan, First-principles molecular dynamics modeling of $UCl_3$ in LiCl–KCl eutectic, 279-286, Copyright 2017, with permission from Elsevier.**

2.230–2.326, 3.024–3.092, and 2.202–2.726 Å, respectively, and the corresponding first CNs were 3.94–4.35, 6.66–7.73, and 6.13–6.35, respectively. A summary of the coordination structures of metal ions in molten chloride salts is shown in Table 2.

### 3.2. Coordination structures of metal ions in fluoride molten salts

With the application of spectral technology and computer simulation technology to characterize the structures of high-temperature molten salts, the research on the microstructures of molten fluoride salt has made some progress, and the research of scholars on the ionic structure of fluoride molten salt systems in recent years is reviewed in this paper.

Bulavin *et al.* [48] investigated the ionic structure of NaF–LiF–$LnF_3$ (Ln = La, Nd) by using a high-temperature XRD technique and concluded that Ln was present in the form of $LnF_4^-$ complexes. Cui *et al.* [49] studied the ionic structure present in the $LaF_3$–LiF molten salt system by applying MD and concluded that the $LaF_6^{3-}$ anion cluster was

**Table 2. Summary of the coordination structures of metal ions in molten chloride salts**

| Molten salts | Methods | Results | Refs. |
|---|---|---|---|
| LiCl, KCl, and others | ND and XRD | The average CN of ions was between 4 and 5, and the ions were anisotropic within the first coordination layer. | [36] |
| LiCl | MC | Li–Cl ionic spacing of 2.40 Å and CN of 4.3. | [37] |
| LiCl and NaCl | MMR | Li–Cl in LiCl molten salts had an approximate tetrahedral structure. The CNs of Na–Na, Na–Cl, and Cl–Cl ion pairs were calculated to be (13.0 ± 0.5), 5.8, and (13.0 ± 0.5), respectively. | [38] |
| KCl | XRD | K–Cl had a coordination distance of 3.05 Å and CN of 4.1. | [39] |
| LiCl–KCl and LiCl–KCl–$SmCl_3$ | QC | The CN values of Li–Cl, K–Cl, and Cl–Cl pairs were 4.33, 7.54, and 10.91, and the first shell CN of Sm coordinated by Cl was 6.56. | [41] |
| $ThCl_4$, $ZrCl_4$, and $ThCl_4$–$ZrCl_4$ | Raman | — | [44–45] |
| $LaCl_3$–ACl (A for alkali metal) | XAFS and MD | $LaCl_6^{3-}$, $LaCl_7^{4-}$, $LaCl_8^{5-}$, and $LaCl_9^{6-}$ were present in the $LaCl_3$ molten salt. | [46–47] |
| LiCl–KCl, LiCl–KCl–$UCl_3$ | QC | The CNs of Li–Cl, K–Cl, and Cl–Cl were calculated as 3.97–4.29, 6.69–7.32, and 9.99–11.39, respectively; the CNs of Li–Cl, K–Cl, and U–Cl were calculated to be 3.94–4.35, 6.66–7.73, and 6.13–6.35, respectively. | [42] |

present within this molten salt system. The structure of the $LaF_6^{3-}$ ion cluster underwent some deformation with the changes in the melt temperature or the concentration of $LaF_3$ in the molten salt fraction. However, the CN of La–F was very close and was always between 7.33 and 7.75. Bessada *et al.* [50] investigated LiF–$ThF_4$–$UF_4$ by EXAFS experiments and MD simulations. The structure of the LiF–$ThF_4$ eutectic with 4mol% $UF_4$ is shown in Fig. 3(a). The results revealed a slight increment in the number of free fluoride ions due to the breakdown of the Th–F chain and the increase in the content of the complex $(Th_XU_YF_Z)^{4X+4Y-Z}$ from 0 to 8mol%. In addition, the average CN of Th–F was very close to eight. Rollet *et al.* [51] investigated the ionic structure of lanthanide fluoride molten salts (LiF–$LuF_3$/$LaF_3$) by using HT NMR and EXAFS. They inferred that a strong $LnF_x^{3-x}$ ionophore was present in the LiF–$LnF_3$ molten salt. Stefanidaki *et al.* [52] investigated the ionic structures of LiF–$NdF_3$ by high-temperature Raman technology and concluded that $NdF_6^{3-}$ ionophores existed in LiF–$NdF_3$. Hatem and Gaune-Escard [53] analyzed the ionic structure of the KF–$NdF_3$ molten salt and discovered that $NdF_6^{3-}$ complex ionic groups were present in this molten salt. Hu *et al.* [54] hypothesized that $NdF_6^{3-}$ and $NdF_4^-$ complexed anion clusters were present in LiF–$NdF_3$. Dracopoulos *et al.* [9] utilized high-temperature Raman techniques to study the microstructure of the $NdF_3$–LiF binary melt salt and found that the melted salt also contained ortho-octahedral $NdF_6^{3-}$ complexed anions.

Dai *et al.* [55] investigated the ionic structure and vibrational spectra of LiF–$BeF_2$ molten salts by the DFT method and discovered that the most likely ionic groups present in the molten salt were $BeF_4^{2-}$, $Be_2F_7^{3-}$, and $Be_3F_{10}^{4-}$. Moreover, the average F–Be and Be–Be distances were within the ranges of (1.564 ± 0.100) and (3.025 ± 0.200) Å, respectively, and the CN of F–Be was maintained at 4. He *et al.* [35] investigated the microstructure of LiF–$BeF_2$ molten salts by MD. The LiF–$BeF_2$ molten salt was observed to mainly consist of a network structure formed by the tetrahedral structure $BeF_4^{2-}$ and the aggregation of $Li^+$. Multiple $BeF_4^{2-}$ formed Be–F–Be bonds through point sharing, yielding structures, such as $Be_2F_7^{3-}$ and $Be_3F_{10}^{4-}$. In addition, the Be–F ion pair had an average first peak radius of 1.58 Å and a CN of 4; the results obtained were consistent with the findings of Dai *et al.* [55].

Lv *et al.* [56] studied the microstructure of LiF–NaF–$AlF_3$ molten salt by using first-principles calculation and discovered that the complex anion groups present in the melt were $AlF_4^-$, $AlF_5^{2-}$, and $AlF_6^{3-}$. Fig. 3(b) shows the local ionic structure in the simulation box for LiF–NaF–$AlF_3$ molten salt with 9wt% LiF. Guo *et al.* [57] applied First principles molecular dynamics (FPMD) to investigate the ionic structure and electronic properties of the KF–NaF–$AlF_3$ molten salt.

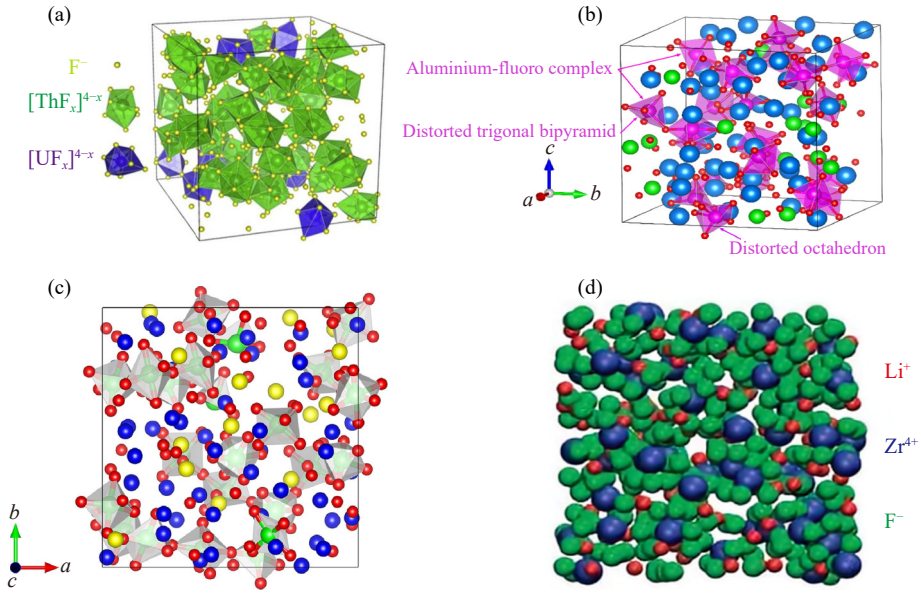


**Fig. 3. Snapshot of the fluoride molten salt structure: (a) atomic configuration of the LiF–$ThF_4$ eutectic with 4mol% $UF_4$ ($Th^{4+}$ in green, $U^{4+}$ in blue, and $F^-$ in red) [50]; (b) the local ionic structure in the simulation box of the LiF–NaF–$AlF_3$ molten salt with 9wt% LiF ($Li^+$ in green, $Na^+$ in blue, $Al^{3+}$ in pink, and $F^-$ in red) [56]; (c) the stable configuration of the KF–NaF–$AlF_3$ system (18wt% KF; $Na^+$ in blue, $K^+$ in yellow, $Al^{3+}$ in green and $F^-$ in red) [57]; (d) the network structure of molten LiF–$ZrF_4$ salts [60]. (a) Reprinted from *J. Mol. Liq.*, 307, C. Bessada, D. Zanghi, M. Salanne, *et al*, Investigation of ionic local structure in molten salt fast reactor LiF-$ThF_4$–$UF_4$ fuel by EXAFS experiments and molecular dynamics simulations, art. No. 112927, Copyright 2020, with permission from Elsevier. (b) Reprinted from *Chem. Phys. Lett.*, 706, C. Bessada, X.J. Lv, Z.X. Han, J.G. Chen, L.X. Jiang, Z.M. Xu, and Q.S. Liu, First-principles molecular dynamics study of ionic structure and transport properties of LiF–NaF–$AlF_3$ molten salt, 237-242, Copyright 2018, with permission from Elsevier. (c) Reprinted from *Chem. Phys. Lett.*, 730, H. Guo, J. Li, H.L. Zhang, *et al.*, First-principles molecular dynamics investigation on KF–NaF–$AlF_3$ molten salt system, 587-593, Copyright 2019, with permission from Elsevier. (d) Reprinted with permission from [O. Pauvert, D. Zanghi, M. Salanne, *et al.*, *J. Phys. Chem. B*, vol. 114, 6472-6479 (2010) [60]]. Copyright 2010 American Chemical Society.**

The configuration is depicted in Fig. 3(c). The results illustrated that the interaction between Al–F was strong and mainly occurred through covalent bonding and formed a large number of $AlF_4^-$, $AlF_5^{2-}$, and $AlF_6^{3-}$ complex ion groups.

Researchers have also conducted some studies on the structure of zirconium in fluoride molten salts, and the structure of $ZrF_4$ in alkali metal fluoride molten salts has been experimentally studied via Raman spectroscopy, NMR, and EXAFS; $ZrF_6^{2-}$, $ZrF_7^{3-}$, and $ZrF_8^{4-}$ were the three main anions present [33–34,58–62]. The network structure of the $LiF–ZrF_4$ molten salt is shown in Fig. 3(d).

In addition, the crystal structure of $K_2TaF_7$, the structure of tantalum fluoride in FLiNaK, belonged to the triangular system with the *P*21/*C* space group [63–65]. The central Ta atom was surrounded by seven fluoride atoms in the form of the $TaF_7^{2-}$ anion. Wang and Duan [66] identified the species of Nb(V) in the FLiNaK melt, and their results indicated that the $NbF_7^{2-}$ complex ion was the dominant ion in the Nb(V)–FLiNaK solution. In the perfluorinated melt, $Ti^{3+}$ or $Ti^{4+}$ was stable in the forms of $TiF_6^{3-}$ and $TiF_6^{2-}$, respectively [67–68]. A summary of coordination structures in molten fluoride salts is shown in Table 3.

### 3.3. Coordination structures of metal ions in nitric acid molten salts

At present, researchers at home and abroad have conducted considerable research on the structure of molten nitrate by using various experimental and computer simulation methods and obtained a series of important conclusions.

Iwadate *et al.* [69] investigated the structures of $NaNO_2$ and $KNO_2$ monosalts by applying the neutron scattering method. The precise analysis of structural parameters, such as CNs, interatomic distances, and temperature factors, yielded the following conclusions. In the presence of stable $NO_2^-$ anions in the melt, the behavior of $NO_2^-$ anions was similar to that of $NO_3^-$ anions due to the presence of lone pairs of electrons. The short-range structure of the $KNO_2$ monosalt was similar to that of $NaNO_2$. However, for the cation ($Na^+/K^+$), its position relative to the anion was slightly different. Fang *et al.* [70–71] studied the microstructure of molten salts, such as $Ca(NO_3)_2$. The radial distribution function of the molten salts was obtained through data processing, and a local structure model of molten salts was constructed to investigate the connection between the melt structure and the crystal growth process. Perelygin and Mikhailov [72] investigated the interaction between ions in nitrate ions by applying infrared and Raman spectroscopy, focusing on ionic association forms.

Berg *et al.* [73] performed a phase diagram study on the $NaNO_2–NaNO_3$ binary system by combining differential scanning calorimetry and Raman spectroscopy. Xu and Chen [74] studied the Raman spectra of the $NaNO_3–KNO_3$ system at different temperatures. Jayaraman *et al.* [75] calculated the thermal properties of Li, Na, and K alkali metal nitrates and the lattice vibrations of $NaNO_2$ by exploiting MD methods.

**Table 3. Summary of coordination structures in fluoride molten salt**

| Molten salt | Method | Results | Refs. |
|---|---|---|---|
| $NaF–LiF–LnF_3$ (Ln = La, Nd) | High-temperature XRD | $LnF_4^-$ existed in the molten salt. | [48] |
| $LaF_3–LiF$ | MD | $LaF_6^{3-}$; the CN of La–F was always between 7.33 and 7.75. | [49] |
| $LiF–ThF_4–UF_4$ | EXAFS and MD | The content of the complex $(Th_XU_YF_Z)^{4X+4Y-Z}$ increased from 0 to 8mol%, and the average CN of Th−F was very close to 8. | [50] |
| $LiF–LuF_3/LaF_3$ | NMR and EXAFS | $LnF_x^{3-x}$ | [51] |
| $LiF–NdF_3$ | High-temperature Raman | $NdF_6^{3-}$ | [52] |
| $KF–NdF_3$ | — | $NdF_6^{3-}$ | [53] |
| $LiF–NdF_3$ | — | $NdF_6^{3-}$ and $NdF_4^-$ | [54] |
| $LiF–NdF_3$ | High-temperature Raman techniques | $NdF_6^{3-}$ | [8] |
| $LiF–BeF_2$ | DFT | $BeF_4^{2-}$, $Be_2F_7^{3-}$, and $Be_3F_{10}^{4-}$ existed in the molten salt; the average F–Be and Be–Be distances were (1.564 ± 0.100) and (3.025 ± 0.200) Å, respectively; and the CN of F−Be was maintained at 4. | [55] |
| $LiF–BeF_2$ | MD | $Be_2F_7^{3-}$, $Be_3F_{10}^{4-}$; the Be−F ion pair had the average first peak radius of 1.58 Å and the CN of 4. | [35] |
| $LiF–NaF–AlF_3$ | MD | $AlF_4^-$, $AlF_5^{2-}$, and $AlF_6^{3-}$ | [56] |
| $KF–NaF–AlF_3$ | QC | $AlF_4^-$, $AlF_5^{2-}$, and $AlF_6^{3-}$ | [57] |
| $ZrF_4$ in alkali metal fluoride melt | Raman, NMR, and EXAFS | $ZrF_6^{2-}$, $ZrF_7^{3-}$, and $ZrF_8^{4-}$ | [33–34, 58–62] |
| $K_2TaF_7–FLiNaK$ | — | Triangular system | [63–65] |
| Nb(V)–FLiNaK | — | $NbF_7^{2-}$ | [66] |
| Perfluorinated melt | — | $TiF_6^{3-}$ and $TiF_6^{2-}$ | [67–68] |

Ponyatenko and Radchenko [76–77] used Raman spectroscopy to study the interaction and rotational motion of $NO_3^-$ ions in $LiNO_3$, $NaNO_3$, $KNO_3$, $RbNO_3$, $CsNO_3$, $AgNO_3$, and $TlNO_3$ monovalent nitrates and monovalent $Ca(NO_3)_2$, $Ba(NO_3)_2$, and $Sr(NO_3)_2$ over a relatively wide temperature range. Gao *et al.* [78] investigated the structure of the binary mixed molten salts of nitrates. The ionic structure of $NaNO_3$–$KNO_3$–$NaNO_2$ molten salts was investigated by Ultra-Violet laser Raman spectroscopy. $NO_3^-$ and $NO_2^-$ were found to be present in the $NaNO_3$–$KNO_3$–$NaNO_2$ molten salt without complex anions. The strength of the N–O bond increased when $NaNO_3$ was added to $KNO_2$–$NaNO_2$.

Zhao *et al.* [79] acquired the structural configurations of the four clusters of $NaNO_3$, $KNO_3$, $NaNO_2$, and $KNO_2$ and Hitec ternary molten salts by applying DFT calculations. Their results revealed that in the microstructures of the four monosalts $NaNO_3$, $KNO_3$, $NaNO_2$, and $KNO_2$, $Na^+/K^+$ and $NO_3^-/NO_2^-$ formed a conformation dominated by monodentate ligands and supplemented by dentate ligands. The higher the content of monodentate ligands, the more stable the molecules. In Hitec mixed molten salts (53wt%$KNO_3$–7wt%$NaNO_3$–40wt%$NaNO_2$), $Na^+$ and $K^+$ were bonded in a single–double dentate mixture, and the structure was more stable when the monodentate content was relatively high and unstable when the double dentate content was relatively high.

### 3.4. Coordination structures of metal ions in molten carbonate salts

As of now, only a few studies on the ionic structure of molten carbonate salts exist. In this paper, the relevant research work of scholars in recent years is discussed.

Hou *et al.* [80] studied the Raman spectra of $Li_2CO_3$, $Na_2CO_3$, and $K_2CO_3$ in solid and molten states at different temperatures (up to 1000°C). The wave number shifts and half-height width changes of the $CO_3^{2-}$ symmetric stretching vibrational modes with the increase in temperature were analyzed.

Chen *et al.* [81] used *in situ* Raman spectroscopy to detect the peroxycarbonate species present in molten carbonates. Their experimental results confirmed that the main oxygen species existing in the $Li/K_2CO_3$ (62:38, mass ratio) molten salt electrolyte under acidic conditions (1 atm $O_2$ + $CO_2$) were $CO_4^{2-}$ or $C_2O_6^{2-}$.

Ohata *et al.* [82] used DFT to derive the structures with the minimum interaction energy of lithium carbonate monomers, dimers, trimers, and tetramers and optimized these structures. Koura *et al.* [83] studied the equilibrium structures of lithium carbonate and potassium carbonate with *ab initio* molecular orbital calculations. Among the four structures of lithium and potassium carbonate, the most stable structure is the one in which all five atoms are in the same plane.

## 4. Factors influencing the structure of molten salt

### 4.1. Effect of temperature on the structure of molten salts

Numerous factors, including temperature, affect the structure of molten salts. This section reviews the effect of current temperature on the molten salt structure.

Wang *et al.* [84] used the MD method to study the effect of temperature on the structure and properties of cryolite and cryolite–alumina molten salt systems. Their results revealed that the CN of F–Al and F–F decreased with the increase in temperature and that the CN of Al–Al first increased and then decreased. Therefore, with the increase in the temperature, the energy of ions in the system increased, the interaction between ions weakened, and mutual attraction between ions was gradually eliminated.

Zhao *et al.* [79] used high-temperature Raman experiments to investigate the effect of temperature on the structure of a molten salt system of nitric acid. Their results revealed that the half-peak widths of the Raman peaks of the mono, di-, and ternary molten salts of $NaNO_3$, $KNO_3$, and $NaNO_2$ increased with the increase in temperature. The effect of temperature on the microstructure of Hitec ternary molten salts was obtained via X-ray scattering experiments. The microstructure of the Hitec molten salt became increasingly unstable as the temperature increased.

Similarly, Hu *et al.* [85] used Raman spectroscopy to study the ionic structures of molten salts at different temperatures. Three Raman characteristic peaks of KF–$KBF_4$ at room temperature were found near 360, 533, and 775 $cm^{-1}$, which were the characteristic Raman peaks of $KBF_4$ corresponding to the $\upsilon_2$, $\upsilon_4$, and $\upsilon_1$ characteristic peaks of $BF_4^-$, respectively. When the mixture melted, the Raman shifts of the three characteristic peaks decreased significantly and further redshifted with the increase in temperature due to the strengthening of the thermal motion of the atoms and the weakening of interatomic forces. In addition, the half-height widths of the above three characteristic peaks increased when the mixture melted due to the increase in the vibrational disorder of the structure.

As can be concluded from the above results, temperature affects the structure of molten salts. As the temperature increases, the thermal motion of atoms intensifies, the structure of each vibrational group loosens; and interatomic forces weaken, resulting in an increase in atomic spacing as well as a broadening of bond angle distribution, an increase in vibrational disorder, and the destabilization of the microstructure of molten salts.

### 4.2. Effect of cations and anions on the structures of molten salts

#### 4.2.1. Effects of cations on structure

The change in composition affects the structures of molten salts to some extent. Therefore, this section first discusses the influence of cations.

Jiang *et al.* [85] studied the form of Sm(III) in molten LiCl–KCl–$SmCl_3$ by Raman spectroscopy. Fig. 4 shows that the Raman spectra of quenched LiCl–KCl salts dissolved diverse amounts of $SmCl_3$ and XRD pattern of quenched salt. In the quenched salt with $SmCl_3$ content less than 5.17mol%, Sm(III) species are mainly $SmCl_6^{3-}$ and a small amount are

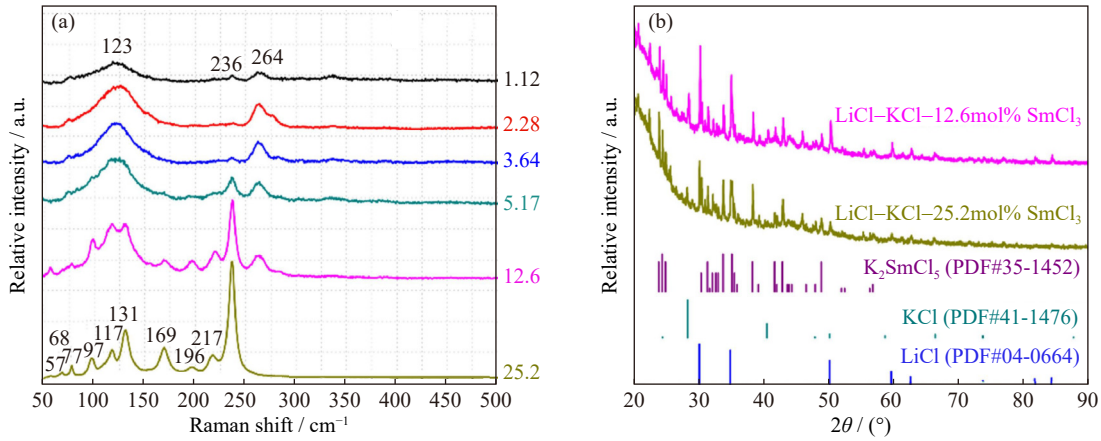


**Fig. 4. (a) Raman spectra of quenched LiCl–KCl salts containing various amounts of $SmCl_3$ at ambient temperature; (b) XRD patterns of quenched LiCl–KCl–$SmCl_3$ salts with $SmCl_3$ molar fractions of 12.6 and 25.2 [85]. Reprinted from *Electrochim. Acta*, 439, S.L. Jiang, C.M. Ye, Y.L. Liu, *et al.*, nsights into the effects of fluoride anions on the electrochemical behavior and solution structure of trivalent samarium in LiCl–KCl molten salt, art. No. 141733, Copyright 2023, with permission from Elsevier.**

$SmCl_7^{4-}$. As the concentration of $SmCl_3$ increases, $SmCl_7^{4-}$ gradually exceeds $SmCl_6^{3-}$ in the melt.

You *et al.* [86] studied the *in situ* Raman spectra of NaF–$AlF_3$ molten salt with different molar ratios (CR = NaF : $AlF_3$) and obtained the types of cluster structures. The law of their variation with composition in high-temperature molten salts was acquired through comparison with theoretical calculations. The molten salt of cryolite (CR = 3.0) contained aluminous fluorine tetrahedra ($Q_2$) with two bridge fluorines in addition to its main structure of isolated aluminous fluorine octahedra ($H_0$). In the molten salt of subcryolite (CR = 1.5), a five-coordinated aluminous fluorine structure type was absent, and although ($H_0$) and ($Q_2$) continued to coexist, their relative content changed. The molten salt of monocryolite (CR = 1.0) showed a significantly changed structure, and isolated aluminous fluorine tetrahedra ($Q_0$) were present with a small amount of aluminous fluorine tetrahedra dimers ($Q_1$). When CR = 0.5, the main structure was dominated by aluminous fluorine tetrahedra dimers ($Q_1$) with a small amount of isolated aluminous fluorine tetrahedra ($Q_0$). These findings indicated that the type of aluminofluorine tetrahedra and the number of bridge fluorines changed with the increase in $AlF_3$ content.

The microstructures of NaCl–KCl and NaCl–RbCl binary mixed molten salts at 827°C were calculated by Wang and Liu [87] by using MD to investigate the effect of NaCl content on the microstructure of molten salts.

In the NaCl–KCl mixed molten salts, the first peak heights of the radial distribution functions between the Na–Cl and K–Cl ions gradually decreased with the gradual increase in NaCl content, and the CNs of Na–Cl and K–Cl gradually increased. The first peak height gradually increased with the increase in NaCl content, and the Cl–Cl ion spacing and CN gradually decreased. The first peak heights of the Na–Na, Na–K, and K–K radial distribution functions decreased slightly with increasing NaCl content, the ion spacing did not show any obvious trend, and the corresponding equivalent CNs gradually increased. In the NaCl–RbCl mixed molten salts, the first peak heights of the Na–Cl and Rb–Cl radial distribution functions decreased gradually with increasing NaCl content, and the ion spacings of Na–Cl and Rb–Cl and their CNs increased gradually with increasing NaCl content.

With the increase in cation content, the ionic spacing and ionic CN between dissimilar ions and cations gradually increased. At the same time, the microscopic arrangement between ions was affected, promoting the close arrangement between dissimilar ions and between cations and inhibiting the close arrangement between anions.

4.2.2. Effects of anions on structures

In titanium molten salts, anions also have a great influence in addition to the cations in molten salt electrolytes that can affect ion morphology and microstructure.

Guo *et al.* [57] used FPMD to study the Al–F bond group and CN in the KF–NaF–$AlF_3$ system at different KF concentrations. Fig. 5 illustrates the Al–F bond population and CN of the system at different KF concentrations. The results indicated that with the increase in KF concentration, the bond population of Al–F first increased and then decreased, which resulted in the same change in the CN of the Al–F complex ion groups.

Hu *et al.* [85] used UV laser Raman spectroscopy to in-

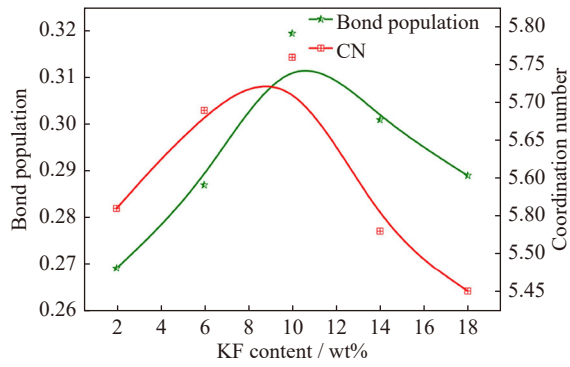


**Fig. 5. Bond population and CN of Al–F in KF–NaF–$AlF_3$ at different KF concentrations [57]. Reprinted from *Chem. Phys. Lett.*, 730, H. Guo, J. Li, H.L. Zhang, *et al.*, First-principles molecular dynamics investigation on KF–NaF–$AlF_3$ molten salt system, 587-593, Copyright 2019, with permission from Elsevier.**

vestigate the effect of the different molar fractions of NaF on the ionic structure of acidic NaF–$AlF_3$ molten salt. Their results demonstrated that the $F^-$ content was low at the measured temperature and intervals of molten salt molar fractions. Furthermore, the molar fraction of $AlF_4^-$ decreased with the increase in the molar fraction of the electrolyte NaF, whereas that of $AlF_6^{3-}$ increased. When the molar fraction of NaF was 0.6, the molar fraction of $AlF_4^-$ was approximately 0.75, whereas that of $AlF_6^{3-}$ was only approximately 0.25. When the molar fraction of NaF increased to 0.71, that of $AlF_4^-$ decreased to approximately 0.25, whereas that of $AlF_6^{3-}$ increased to approximately 0.75. Liu *et al.* [88] investigated the electrochemical behavior and coordination properties of uranium by combining electrochemical and spectral techniques and *ab initio* MD simulations. Their results revealed that $F^-$ ions can more easily coordinate with U(IV) than with U(III) and had a smaller ionic radius and higher charge density. The involvement of $F^-$ ions made the U(IV) complex more stable, and the equilibrium potential of U(IV)/U(III) moved in a negative direction, approaching the equilibrium potential of U(III)/U(0). When $Cl^-$ ions were abundant, $F^-$ ions cannot completely replace the role of $Cl^-$ ions such that U(IV) and U(III) were more inclined to form $UCl_3F_3^{2-}$ and $UCl_5F^{3-}$ complexes, respectively. Wu *et al.* [89] studied the cathodic reduction mechanism of Hf(IV) ions in a molten NaCl–KCl–NaF–$K_2HfF_6$ salt system at different NaF concentrations. $F^-$ gradually replaced $Cl^-$ with the increase in NaF concentration. As a result of the high thermodynamic stability of $HfF_6^{2-}$, $HfCl_mF_n^{2-}$ ($m + n = 6$) was transformed into $HfF_6^{2-}$.

Our team has also done considerable research on the influence of $F^-$ on molten salt structures. Song *et al.* [90] added KF as a fluoride ion source to NaCl–KCl–$TiCl_4$ molten salt. They found that almost all $Ti^{3+}$ and $Ti^{4+}$ formed coordination complexes and the CN equaled 6, $TiF_6^{3-}$ and $TiF_6^{2-}$ in high-concentration fluoride melt. By applying a combination of spectral, electrochemical, and mathematical analyses, Liu *et al.* [91] investigated the effect of $F^-$ on the electrochemical behavior and coordination characteristics of titanium ions. They also performed Raman spectral analysis on samples with different proportions. The results are provided in Fig. 6, which illustrates that $F^-$ can reduce the reduction steps of titanium ions and affect the proportion of the valence states of titanium ions. Raman analysis and X-ray photoelectron spectroscopy (XPS) results revealed that fluoride ions formed $TiCl_jF_i^{m-}$ with titanium ions in molten salts containing titanium ions.

Yuan *et al.* [92] used XPS and Raman to analyze the complexes in LiCl–KCl eutectic salts containing $VCl_3$ and KF. They demonstrated that when fluoride was added to the molten salt, the V–Cl bond was replaced by the V–F bond and combined with V(III) to form $VF_6^{3-}$, as shown in Fig. 7. Moreover, with the addition of fluoride ions, the particle size of the product decreased. Bai *et al.* [93] revealed the chemical coordination mechanism of tantalum ions in the above molten salts. When fluoride ions were added to the

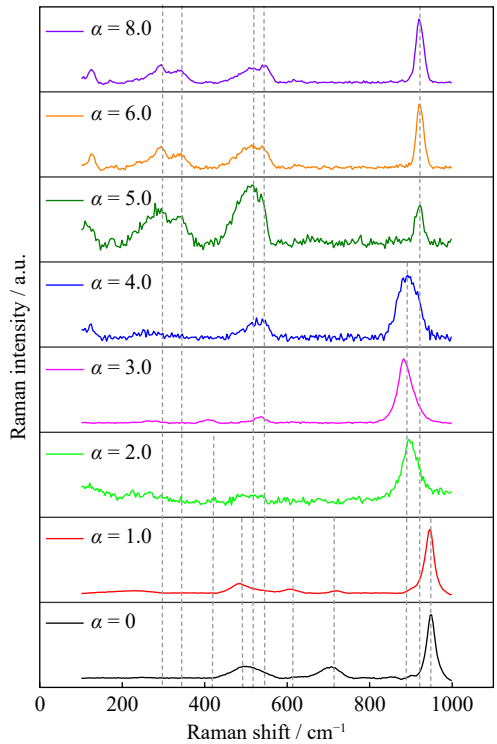


**Fig. 6. Raman spectra of samples under different $\alpha$ (molar ratios of $[F^-]/[Ti^{n+}]$) conditions [91]. Reprinted by permission from Springer Nature: *Int. J. Miner. Metall. Mater.*, Effect of fluoride ions on coordination structure of titanium in molten NaCl–KCl, S.S. Liu, S.L. Li, C.H. Liu, J.L. He, and J.X. Song, Copyright 2023.**

NaCl–KCl–$TaCl_5$ molten salt, the Ta–Cl bond in the system was gradually replaced by the Ta–F bond such that the tantalum and fluoride ions in the molten salt formed a new complex, namely, $TaCl_xF_y^{n-}$, with stronger stability. Finally, $TaF_y^{n-}$ was formed.

$F^-$ is a single base ligand with a stronger coordination ability than $Cl^-$. The addition of $F^-$ to the chloride molten salt will result in coordination substitution and change the coordination structure of ions in the molten salt to form fluoro–chloride. The fluorine-containing ligand is stronger than the chlorine-containing ligand and has a more stable structure.

### 4.3. Effect of $O^{2-}$ on the structure of molten salts

The influence of oxygen ions on the structure and properties of molten salt has rarely been reported. Therefore, this section summarizes the influence of the addition of oxygen ions on the structure of molten salts.

Guo *et al.* [94] directly studied the ion microstructure of the KF–NaF–$AlF_3$–$Al_2O_3$ system by using FPMD. Their results indicated that with the increase in $Al_2O_3$ concentration, Al–F–Al, Al–O–Al, and Al–O–F formed complex ion groups, and the ion microstructure of the system became more complex.

Wang and Duan [66] investigated the effect of $O^{2-}$ on the structure of molten salts by adding $Na_2O$ to $K_2NbF_7$–FLiNaK and showed that $NbOF_6^{3-}$ is a stable monooxyfluoro complex anion present in FLiNaK. The number of $NbOF_6^{3-}$ species in-

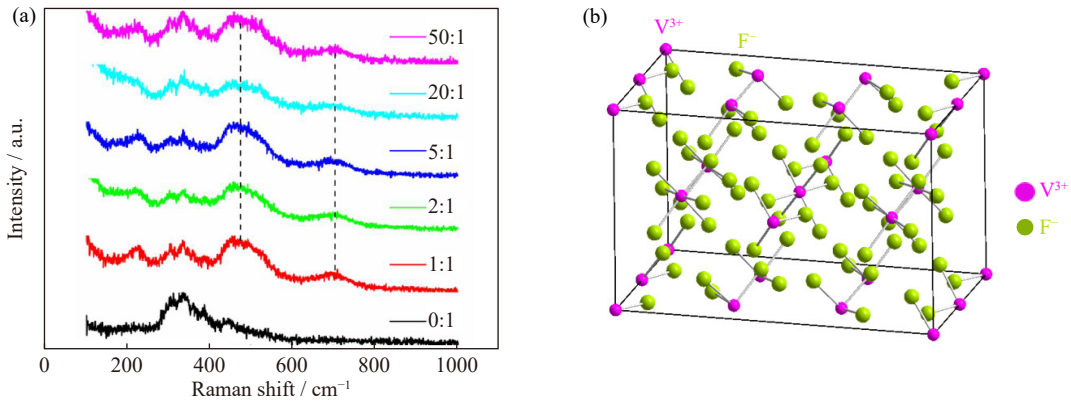


**Fig. 7. (a) Raman spectra of $VCl_3$ in LiCl–KCl–KF molten salt with various molar ratios of $[F^-]/[V^{n+}]$; (b) the geometric structure of $VF_6^{3-}$ [92]. Reprinted from *Trans. Monferrous Met. Soc. China*, 32, R. Yuan, C. Lü, H.L. Wan, *et al.*, Effect of fluoride addition on electrochemical behaviors of V(III) in molten LiCl−KCl, 2736-2745, Copyright 2022, with permission from Elsevier.**

creased with the increase in $O^{2-}$ when the molar ratio of $O^{2-}$/Nb(V) was less than 1.0. Wang *et al.* [95] investigated the effect of $O^{2-}$ on the structure of metal fluorides with the addition of $Li_2O$ by applying a combination of Raman spectroscopy and QC theoretical calculations. Their results showed that for vanadium group elements, the addition of $Li_2O$ resulted in the formation of $TaOF_5^{2-}$/$NbOF_5^{2-}$ and $TaOF_6^{3-}$/$NbOF_6^{3-}$ structures and the depletion of $TaF_7^{2-}$/$NbF_7^{2-}$ and $TaF_8^{3-}$/$NbF_8^{3-}$ fluoride structures.

Chen *et al.* [96] used Raman spectroscopy to study the effect of oxide ions on the morphology of KF molten liquid containing $ZrF_4$ and $HfF_4$. Zirconium and hafnium fluoride existed in the forms of $MF_6^{2-}$ and $MF_7^{3-}$ (M = Zr, Hf) in KF melts with lower $MF_4$ concentrations, whereas $MF_6^{2-}$ was dominant at higher $MF_4$ concentrations. When 3mol%–5mol% $Li_2O$ was added to KF–$MF_4$ (10mol%) melt, $MOF_5^{3-}$ formed oxyfluorides with characteristic terminal M–O stretching bands at 775 (Zr) and 763 (Hf) $cm^{-1}$. However, when 5mol% $Li_2O$ was added to the KF melt containing 30mol%–40mol% $ZrF_4$ and $HfF_4$, these fluoroxides were not observed. Consistent with the formation of $MOF_5^{3-}$, the mean binding energy of $MF_7^{3-}$ was considerably lower than that of $MF_6^{2-}$.

Wang *et al.* [97] investigated the effect of $Nd_2O_3$ on the properties and structure of an $AlF_3$–(Na/Li)F–$Al_2O_3$ melt by measuring the density, viscosity, and conductivity of the molten salt system by applying the Archimedes, rotational, and continuously varying conductivity cell constants methods. Their results showed that the addition of $Nd_2O_3$ increased the ionic gap of the system and produced ionic groups with low stacking density. In addition, the introduction of $Nd^{3+}$ may lead to the formation of the Nd–O–F complex ion groups $NdOF_3^{2-}$, $NdOF_5^{4-}$, $Nd_2OF_6^{2-}$, $Nd_2OF_8^{4-}$, and $Nd_2OF_4^{2-}$ as a result of the substitution reaction with the existing Al–O–F in the molten salt.

Liu *et al.* [98] studied the microstructure of fused FLiNaK–$LuF_3$ and FLiNaK–$LuF_3$–$Li_2O$ systems by combining Raman spectroscopy and density functional theory calculations. The anion $Lu_2OF_8^{4-}$ was formed by the addition of $Li_2O$ to molten FLiNaK–$LuF_3$ (20mol%), which has a linear Lu–O–Lu geometry with one oxygen atom bridging two $LuF_4$ groups. When the content of $Li_2O$ was 10mol%, $Lu_2O_2F_4^{2-}$ and $Lu_2O_2F_6^{4-}$ were formed.

In summary, the above researchers studied the effects of metal oxides ($O^{2-}$) on molten salt systems by employing spectroscopic techniques and computer simulations. Their results demonstrated that in molten salts, complex oxygen ions changed the structure of the molten salts with the addition of metal oxides ($O^{2-}$). This finding provides a theoretical basis for clarifying the electrolytic mechanism. The influence of cations and anions on the structural aspects of molten salts is summarized in Table 4, and the influence of $O^{2-}$ on the structural aspects of molten salts is shown in Table 5.

## 5. Conclusions and outlook

The molten salt structure is of crucial importance as the foundation for the study of molten salt theory. Nevertheless, it is difficult to obtain because microstructures cannot be investigated directly by experimental means and can only be described qualitatively on the basis of experimental data. However, with the continuous improvement in simulation algorithms and the increasing development of computer technology, computer simulation techniques, which are represented by MD simulations, have emerged and are widely used. Studying the interaction between system particles and the microstructures of molten salts by using MD simulation technologies, which can simulate the behavior of real fluids, is possible. In this paper, a variety of characterization methods for studying the structure of molten salts are listed. These methods mainly included XRD, Raman, NDT, NMR, EXAFS, electrochemical analysis, and computer simulation. At the same time, the results of existing research on the system structures of chloride salt, fluoride salt, nitrate, and molten carbonate salt were introduced.

The effects of temperature, anions and cations, and metal oxides ($O^{2-}$) on the structure of molten salts are summarized below.

(1) The increment in temperature loosens the structure of molten salts. With the increase in temperature, the thermal

**Table 4. Influence of cations and anions on the structural aspects of molten salts**

| Ion | | Molten salt | Method | Main conclusion | Ref. |
|---|---|---|---|---|---|
| Cation | $Sm^{3+}$ | LiCl–KCl– $SmCl_3$ | Raman, XRD | As the concentration of $SmCl_3$ increases, $SmCl_7^{4-}$ gradually exceeds $SmCl_6^{3-}$ in the melt. | [85] |
| | $Al^{3+}$ | NaF–$AlF_3$ | *In situ* Raman | CR = 3.0: $H_0$, $Q_2$; CR = 1.5: coexistence of $H_0$ and $Q_2$; CR = 1.0: $Q_0$, mainly; a small amount of $Q_1$; CR = 0.5: $Q_1$, mainly; a small amount of $Q_0$. | [86] |
| | $Na^+$ | NaCl –KCl | MD | The CN of Na–Cl and K–Cl gradually increased; the Cl–Cl ion spacing and CN gradually decreased; the corresponding equivalence CN gradually increased. | [87] |
| | $Na^+$ | NaCl –RbCl | MD | Na–Cl and Rb–Cl ion spacing and CN gradually increased; Cl–Cl ion spacing and CN gradually decreased; Na–Na, Na–Rb, and Rb–Rb ion spacing had no obvious trend. | [87] |
| Anion | $F^-$ | KF–NaF–$AlF_3$ | MD | With the increase in KF concentration; the bond population of Al–F first increased and then decreased; the same change of CN of Al–F complex ion groups. | [57] |
| | $F^-$ | NaF–$AlF_3$ | UV, Raman | The molar fraction of $AlF_4^-$ decreased with the increase in the molar weight fraction of the electrolyte NaF, whereas the molar fraction of $AlF_6^{3-}$ increased. | [85] |
| | $F^-$ | LiCl–KCl–$UCl_4$–LiF | MD | $F^-$ ion easily coordinated with U(IV), its ionic radius was smaller, and its charge density was higher. When $Cl^-$ ions were abundant, U(IV) and U(III) were more inclined to form $UCl_3F_3^{2-}$ and $UCl_5F^{3-}$ complexes, respectively. | [88] |
| | $F^-$ | NaCl–KCl–NaF–$K_2HfF_6$ | CV, SWV, and XRD | With the increase in NaF concentration, [$F^-$] gradually replaced [$Cl^-$], and [$HfCl_mF_n^{2-}$] ($m + n = 6$)] transformed into [$HfF_6^{2-}$]. | [89] |
| | $F^-$ | NaCl–KCl–$TiCl_4$–KF | — | In high-concentration fluoride melts, almost all $Ti^{3+}$ and $Ti^{4+}$ formed coordination complexes, and CN = 6. | [90] |
| | $F^-$ | $Ti^{2+}$/$Ti^{3+}$/$Ti^{4+}$–NaCl–KCl–KF | EC, mathematical analysis, and spectral techniques | $F^-$ shortened the reduction step of titanium ions and affected the proportion of the valence states of titanium ions. Fluoride ions and titanium ions formed $TiCl_jF_i^{m-}$ in molten salt. | [91] |
| | $F^-$ | LiCl–KCl–$VCl_3$–KF | XPS and Raman | With the addition of fluoride ions, the V–Cl bond was replaced by the V–F bond and combined with V(III) to form $VF_6^{3-}$, and the particle size of the product decreased. | [92] |
| | $F^-$ | NaCl–KCl–$TaCl_5$–NaF | XPS and Raman | The Ta–Cl bond in the system was replaced by the Ta–F bond, and tantalum and fluoride ions formed the new complex $TaCl_xF_y^{n-}$ with stronger stability, then $TaF_y^{n-}$ formed. | [93] |

motion of atoms strengthens, interatomic forces weaken, vibrational disorder increases, and the microstructures of molten salts destabilize.

(2) The increase of cation content in the composition of molten salt affects the microscopic arrangement between ions, which makes the arrangement between different ions and cations closer but also inhibits the tight arrangement between anions. It also changes the structural types of clusters in molten salts. Anions also affect the structure of molten salts. Given the strong coordination ability of $F^-$, $F^-$ addition leads to coordination substitution in the molten chlorine salt and changes the coordination structure of the clusters in the molten salt. Considering that the coordination bond strength of fluorine is greater than that of chlorine, the structure of fluorine is also more stable.

(3) With the increase in metal oxide ($O^{2-}$) concentration, more complex oxygen-containing ions form in molten salt. This effect will change the composition and properties of the molten salt.

Studies on the microstructure of molten salts have not yet reached a consensus, particularly regarding complex molten salt systems, such as complex mixture systems that involve multibody interactions. This situation requires more abundant research tools and more research work. Any kind of structural research method only reflects the side of the overall structural information of matter and gradually improves with its development. Thus, combining theoretical and experimental methods as well as different methods in theory

**Table 5. Influence of $O^{2-}$ on the structural aspects of molten salts**

| Molten salt | Oxides form | Method | Main conclusion | Ref. |
|---|---|---|---|---|
| $KF–NaF–AlF_3–Al_2O_3$ | $Al_2O_3$ | FPMD | With the increase in $Al_2O_3$ concentration, Al–F–Al, Al–O–Al, and Al–O–F formed complex ion groups. | [94] |
| $K_2NbF_7$–FLiNaK | $Na_2O$ | — | $NbOF_6^{3-}$ was a stable mono-oxyfluoro complex anion present in FLNAK, and the number of $NbOF_6^{3-}$ species increased with the increase in $O^{2-}$. | [66] |
| FLiNaK–$K_2TaF_7$/$K_2NbF_7$ | $Li_2O$ | Raman and QC theoretical calculations | $TaOF_5^{2-}$/$NbOF_5^{2-}$ and $TaOF_6^{3-}$/$NbOF_6^{3-}$ formed, and $O^{2-}$ caused the polymerization of fluorine oxides in the molten salt and the appearance of solid immiscible material, forming an oxide-like structure. | [95] |
| $KF–ZrF_4/HfF_4$ | $Li_2O$ | Raman | $MOF_5^{3-}$ was observed. Raman bands formed by zirconium and hafnium oxides were formed. | [96] |
| $AlF_3$–(Na/Li)F–$Al_2O_3$ | $Nd_2O_3$ | Spectroscopy and MD | $Nd_2O_3$ led to the increase in the ionic gap of the system and the generation of ionic groups with small stacking density. $NdOF_3^{2-}$, $NdOF_5^{4-}$, $Nd_2OF_6^{2-}$, $Nd_2OF_8^{4-}$, and $Nd_2OF_4^{2-}$ formed. | [97] |
| FLiNaK–$LuF_3$–$Li_2O$ | $Li_2O$ | Raman and DFT | $Lu_2OF_8^{4-}$ formed, and $Lu_2O_2F_4^{2-}$ and $Lu_2O_2F_6^{4-}$ formed when more $Li_2O$ was added. | [98] |

and experiments is necessary to obtain relatively complete microstructure information. The multiscale analysis and characterization of molten salt structures can be carried out by combining various *in situ* and non-*in situ* techniques to explore the microstructure and coordination of molten salts deeply. In the future, more accurate and intuitive molten salt structures can be revealed with the aid of evolving scientific and technological methods.

## Acknowledgements

This work was financially supported by the National Key Research and Development Program of China (Nos. 2021YFC2901600 and 2021YFC2902305), the National Natural Science Foundation of China (No. 52274356), the Natural Science Foundation of Henan Province, China (No. 222300420545), the State Key Laboratory of Special Rare Metal Materials, China (No. SKL2020K004), the Northwest Rare Metal Materials Research Institute, China, and the State Key Laboratory of Complex Nonferrous Metal Resources Clean Utilization, China (No. CNMRCUKF2008).

## Conflict of Interest

The authors declare no conflict of interest.

## References

[1] S.Q. Jiao, M.Y. Wang, and W.L. Song, Editorial for special issue on high-temperature molten salt chemistry and technology, *Int. J. Miner. Metall. Mater.*, 27(2020), No. 12, p. 1569.

[2] X.L. Xi, M. Feng, L.W. Zhang, and Z.R. Nie, Applications of molten salt and progress of molten salt electrolysis in secondary metal resource recovery, *Int. J. Miner. Metall. Mater.*, 27(2020), No. 12, p. 1599.

[3] V. van Speybroeck, R. Gani, and R.J. Meier, The calculation of thermodynamic properties of molecules, *Chem. Soc. Rev.*, 39(2010), No. 5, p. 1764.

[4] W. Jia, *Molecular Dynamics Study on Structure and Properties of Molten Salt in Alkali Metal Chloride System* [Dissertation], East China University of Science and Technology, Shanghai, 2016, p. 145.

[5] M.H. Brooker, R.W. Berg, J.H. von Barner, and N.J. Bjerrum, Matrix-isolated $Al_2OF_6^{2-}$ ion in molten and solid LiF/NaF/KF, *Inorg. Chem.*, 39(2000), No. 21, p. 4725.

[6] Y.J. Jin and Y.B. Ai, The technology of nuclear magnetic resonance and its applications, *Phy. Eng.*, 12(2002), No. 1, p. 47.

[7] Y. Iwadate, K. Suzuki, N. Onda, *et al.*, Local structure of molten $LaCl_3$ analyzed by X-ray diffraction and La–$L_{III}$ absorption-edge XAFS technique, *J. Alloys Compd.*, 408-412(2006), p. 248.

[8] C.Y. Wang, X.T. Chen, R. Wei, and Y. Gong, Raman spectroscopic and theoretical study of scandium fluoride and oxyfluoride anions in molten FLiNaK, *J. Phys. Chem. B*, 124(2020), No. 30, p. 6671.

[9] V. Dracopoulos, B. Gilbert, and G.N Papatheodorou, Vibrational modes and structure of lanthanide fluoride-potassium fluoride binary melts $LnF_3$–KF (Ln = La, Ce, Nd, Sm, Dy, Yb), *J. Chem. Soc., Faraday Trans.*, 94(1998), No. 17, p. 2601.

[10] N. Ma, J.L. You, L.M. Lu, J. Wang, M. Wang, and S.M. Wan, Micro-structure studies of the molten binary $K_3AlF_6$–$Al_2O_3$ system by *in situ* high temperature Raman spectroscopy and theoretical simulation, *Inorg. Chem. Front.*, 5(2018), No. 8, p. 1861.

[11] F.G. Edwards, J.E. Enderby, R.A. Howe, and D.I. Page, The structure of molten sodium chloride, *J. Phys. C Solid State Phys.*, 8(1975), No. 21, p. 3483.

[12] E.W.J. Mitchell, P.F.J. Poncet, and R.J. Stewart, The ion pair distribution functions in molten rubidium chloride, *Philos. Mag.*, 34(1976), No. 5, p. 721.

[13] J. Locke, S. Messoloras, R.J. Stewart, R.L. McGreevy, and E.W.J. Mitchell, The structure of molten CsCl, *Philos. Mag. B*, 51(1985), No. 3, p. 301.

[14] X.M. Liu, H.H. Sun, X.P. Feng, and N. Zhang, Relationship between the microstructure and reaction performance of aluminosilicate, *Int. J. Miner. Metall. Mater.*, 17(2010), No. 1, p. 108.

[15] A.L. Rollet, C. Bessada, A. Rakhmatoulline, *et al., In situ* high temperature NMR and EXAFS experiments in rare-earth fluoride molten salts, *C. R. Chim.*, 7(2004), No. 12, p. 1135.
[16] A.L. Rollet, E. Veron, and C. Bessada, Fission products behavior in molten fluoride salts: Speciation of $La^{3+}$ and $Cs^{+}$ in melts containing oxide ions, *J. Nucl. Mater.*, 429(2012), No. 1-3, p. 40.
[17] A.L. Rollet and M. Salanne, Studies of the local structures of molten metal halides, *Annu. Rep. Prog. Chem., Sect. C: Phys. Chem.*, 107(2011), p. 88.
[18] Y. Okamoto, H. Shiwaku, T. Yaita, S. Suzuki, and M. Gaune-Escard, High-energy EXAFS study of molten $GdCl_3$ systems, *J. Mol. Liq.*, 187(2013), p. 94.
[19] Y. Okamoto, XAFS simulation of highly disordered materials, *Nucl. Instrum. Methods Phys. Res. Sect. A*, 526(2004), No. 3, p. 572.
[20] Y. Okamoto, H. Shiwaku, T. Yaita, H. Narita, and H. Tanida, Local structure of molten $LaCl_3$ by K-absorption edge XAFS, *J. Mol. Struct.*, 641(2002), No. 1, p. 71.
[21] G.D. Zissi, A. Chrissanthopoulos, and G.N. Papatheodorou, Vibrational modes and structure of the $LaCl_3$–CsCl melts, *Vib. Spectrosc.*, 40(2006), No. 1, p. 110.
[22] G. Bontempelli, F. Magno, and S. Daniele, Simple relationship for calculating backward to forward peak-current ratios in cyclic voltammetry, *Anal. Chem.*, 57(1985), No. 7, p. 1503.
[23] J.J. O'Dea, J. Osteryoung, and R.A. Osteryoung, Theory of square wave voltammetry for kinetic systems, *Anal. Chem.*, 53(1981), No. 4, p. 695.
[24] F. Lantelme and M. Chemla, Chronoamperometry for the determination of metallic interdiffusion coefficients. Rapid transport processes in the first atomic layers, *J. Electroanal. Chem.*, 396(1995), No. 1-2, p. 203.
[25] T.J. Zhu, C.Y. Wang, H.Y. Fu, W. Huang, and Y. Gong, Electrochemical and Raman spectroscopic investigations on the speciation and behavior of chromium ions in fluoride doped molten LiCl–KCl, *J. Electrochem. Soc.*, 166(2019), No. 10, p. H463.
[26] M.Y. Wu, *Dissolution and Electrochemical Reduction of Multivalent Refractory Metal Oxides in NaKClF Molten Salt* [Dissertation], North China University of Science and Technology, Tangshan, 2016, p. 85.
[27] J. Hetmańczyk, Ł. Hetmańczyk, A. Migdał-Mikuli, and E. Mikuli, Vibrational and reorientational dynamics, crystal structure and solid–solid phase transition studies in $[Ca(H_2O)_6]Cl_2$ supported by theoretical (DFT) calculations, *J. Raman Spectrosc.*, 47(2016), No. 5, p. 591.
[28] Y.C. Chen, Principle and application of quantum chemical computation, *Technol. Manage. Sci.*, (2020), p. 110.
[29] X.J. Li, J. Song, S.P. Shi, *et al*., Dynamic fluctuation of $U^{3+}$ coordination structure in the molten LiCl–KCl eutectic via first principles molecular dynamics simulations, *J. Phys. Chem. A*, 121(2017), No. 3, p. 571.
[30] N. Metropolis and S. Ulam, The Monte Carlo method, *J. Am. Stat. Assoc.*, 44(1949), No. 247, p. 335.
[31] A. Baranyai, I. Ruff, and R.L. McGreevy, Monte Carlo simulation of the complete set of molten alkali halides, *J. Phys. C: Solid State Phys.*, 19(1986), No. 4, p. 453.
[32] B.J. Alder and T.E. Wainwright, Studies in molecular dynamics. I. General method, *J. Chem. Phys.*, 31(1959), No. 2, p. 459.
[33] C. Bessada, O. Pauvert, D. Zanghi, *et al., In situ* experimental approach of the speciation in molten lanthanide and actinide fluorides combining NMR, EXAFS and molecular dynamics, *ECS Trans.*, 33(2010), No. 7, p. 361.
[34] C. Bessada, O. Pauvert, L. Maksoud, *et al.*, *In situ* experimental approach of speciation in molten fluorides: A combination of NMR, EXAFS, and molecular dynamics, [in] M. Gaune-Escard and G.M. Haarberg eds., *Molten Salts Chemistry Technololgy*, Weley, 2014, p. 219.
[35] G.D. He, R. Tang, X.Z. Duan, *et al*., Molecular dynamics study on microstructure and diffusion characteristics of LiF–$BeF_2$ molten salt, *Chem. Eng. J.*, 71(2020), No. 8, p. 3565.
[36] H.A. Levy, P.A. Agron, M.A. Bredig, and M.D. Danford, X-ray and neutron diffraction studies of molten alkali halides, *Ann. N. Y. Acad. Sci.*, 79(1960), No. 11, p. 762.
[37] T. Førland, T. Østvold, J. Krogh-Moe, Monte Carlo studies on fused salts. I. Calculations for a two-dimensional ionic model liquid, *Acta Chem. Scand.*, 22(1968), No. 8, p. 2415.
[38] M.A. Howe and R.L. McGreevy, A neutron-scattering study of the structure of molten lithium chloride, *Philos. Mag. B*, 58(1988), No. 5, p. 485.
[39] R. Takagi, H. Ohno, and K. Furukawa, Structure of molten KCl, *J. Chem. Soc., Faraday Trans. 1*, 75(1979), art. No. 1477.
[40] C. Kwon, S.H. Noh, H. Chun, I.S. Hwang, and B. Han, First principles computational studies of spontaneous reduction reaction of Eu(III) in eutectic LiCl–KCl molten salt, *Int. J. Energy Res.*, 42(2018), No. 8, p. 2757.
[41] J. Zhao, Z.T. Liu, W.S. Liang, and G.M. Lu, Evaluation of the local structure and electrochemical behavior in the LiCl–KCl–$SmCl_3$ melt, *J. Mol. Liq.*, 363(2022), art. No. 119818.
[42] J. Song, S.P. Shi, X.J. Li, and L.M. Yan, First-principles molecular dynamics modeling of $UCl_3$ in LiCl–KCl eutectic, *J. Mol. Liq.*, 234(2017), p. 279.
[43] T. Jiang, N. Wang, C.M. Cheng, S.M. Peng, and L.M. Yan, Molecular dynamics simulation on the structure and thermodynamics of molten LiCl–KCl–$CeCl_3$, *Acta Phys. Chim. Sin.*, 32(2016), No. 3, p. 647.
[44] G. Pastore, Z. Akdeniz, and M.P. Tosi, Structure of molten yttrium chloride in an ionic model, *J. Phys. Condens. Matter*, 3(1991), No. 42, p. 8297.
[45] Z. Akdeniz and M.P. Tosi, Structure and binding of ionic clusters in Th and Zr chloride melts, *Z. Naturforsch. A: Phys. Sci.*, 56(2001), No. 11, p. 717.
[46] Y. Okamoto and P.A. Madden, Structural study of molten lanthanum halides by X-ray diffraction and computer simulation techniques, *J. Phys. Chem. Solids*, 66(2005), No. 2-4, p. 448.
[47] Y. Okamoto, S. Suzuki, H. Shiwaku, A. Ikeda-Ohno, T. Yaita, and P.A. Madden, Local coordination about $La^{3+}$ in molten $LaCl_3$ and its mixtures with alkali chlorides, *J. Phys. Chem. A*, 114(2010), No. 13, p. 4664.
[48] L. Bulavin, V. Sokol'skii, O. Roik, *et al*., Structure and physical properties of ternary NaF–LiF–$LnF_3$ (Ln = La, Nd) systems of eutectic compositions, *Phys. Chem. Liq.*, 54(2016), No. 6, p. 717.
[49] H. Cui, *Molecular Dynamics Simulation of Melt Structure of Rare Earth Metal Halide Molten Salt System* [Dissertation], Kunming University of Science and Technology, 2002, Kumming, p. 136.
[50] C. Bessada, D. Zanghi, M. Salanne, *et al*., Investigation of ionic local structure in molten salt fast reactor LiF–$ThF_4$–$UF_4$ fuel by EXAFS experiments and molecular dynamics simulations, *J. Mol. Liq.*, 307(2020), art. No. 112927.
[51] A.L Rollet, A. Rakhmatullin, and C. Bessada, Local structure analogy of lanthanide fluoride molten salts, *Int. J. Thermophys.*, 26(2005), No. 4, p. 1115.
[52] E. Stefanidaki, G.M. Photiadis, C.G. Kontoyannis, A.F. Vik, and T. Østvold, Oxide solubility and Raman spectra of $NdF_3$–LiF–KF–$MgF_2$–$Nd_2O_3$ melts, *J. Chem. Soc., Dalton*

*Trans.*, 2002, No. 11, p. 2302.
[53] G. Hatem and M. Gaune-Escard, Calorimetric investigation of $\{xKF^{+}(1-x)NdF_3\}$(l), *J. Chem. Thermodyn.*, 25(1993), No. 2, p. 219.
[54] X.W. Hu, Z.W. Wang, B.L. Gao, Z.N. Shi, F.G. Liu, and X.Z. Cao, Density and ionic structure of $NdF_3$–LiF melts, *J. Rare Earths*, 28(2010), No. 4, p. 587.
[55] J.X. Dai, H. Han, Q.N. Li, and P. Huai, First-principle investigation of the structure and vibrational spectra of the local structures in LiF–$BeF_2$ molten salts, *J. Mol. Liq.*, 213(2016), p. 17.
[56] X.J. Lv, Z.X. Han, J.G. Chen, L.X. Jiang, Z.M. Xu, and Q.S. Liu, First-principles molecular dynamics study of ionic structure and transport properties of LiF–NaF–$AlF_3$ molten salt, *Chem. Phys. Lett.*, 706(2018), p. 237.
[57] H. Guo, J. Li, H.L. Zhang, *et al*., First-principles molecular dynamics investigation on KF–NaF–$AlF_3$ molten salt system, *Chem. Phys. Lett.*, 730(2019), p. 587.
[58] C. Bessada, D. Zanghi, O. Pauvert, *et al*., High temperature EXAFS experiments in molten actinide fluorides: The challenge of a triple containment cell for radioactive and aggressive liquids, *J. Nucl. Mater.*, 494(2017), p. 192.
[59] Y. Qiao, C.M. Pedersen, Y.X. Wang, and X.L. Hou, NMR insights on the properties of $ZnCl_2$ molten salt hydrate medium through its interaction with $SnCl_4$ and fructose, *ACS Sustainable Chem. Eng.*, 2(2014), No. 11, p. 2576.
[60] O. Pauvert, D. Zanghi, M. Salanne, *et al., In situ* experimental evidence for a nonmonotonous structural evolution with composition in the molten LiF–$ZrF_4$ system, *J. Phys. Chem. B*, 114(2010), No. 19, p. 6472.
[61] C. Bessada and A.L. Rollet, *In situ* spectroscopy in molten fluoride salts, [in] F. Lantelme and H. Grou eds., *Molten Salts Chemistry*, Elsevier, 2013, p. 33.
[62] O. Pauvert, M. Salanne, D. Zanghi, *et al*., Ion specific effects on the structure of molten AF–$ZrF_4$ systems ($A^+$ = $Li^+$, $Na^+$, and $K^+$), *J. Phys. Chem. B*, 115(2011), No. 29, p. 9160.
[63] J.L. Hoard, Structures of complex Fluorides.1 Potassium heptafluocolumbate and potassium heptafluotantalate. The configuration of the heptafluocolumbate and heptafluotantalate ions, *J. Am. Chem. Soc.*, 61(1939), No. 5, p. 1252.
[64] R.B. English, A.M. Heyns, and E.C. Reynhardt, An X-ray, NMR, infrared and Raman study of $K_2TaF_7$, *J. Phys. C Solid State Phys.*, 16(1983), No. 5, p. 829.
[65] C.C. Torardi, L.H. Brixner, and G. Blasse, Structure and luminescence of $K_2TaF_7$ and $K_2NbF_7$, *J. Solid State Chem.*, 67(1987), No. 1, p. 21.
[66] X.D. Wang and S.Z. Duan, Identification of complex ions of Nb(V) in FLINAK–$O^{2-}$ System by infrared spectra, *Rare Met.*, 12(1993), No. 3, p. 209.
[67] G.S. Chen, M. Okido, and T. Oki, Electrochemical studies of titanium ions ($Ti^{4+}$) in equimolar KCl–NaCl molten salts with 1 wt% $K_2TiF_6$, *Electrochim. Acta*, 32(1987), No. 11, p. 1637.
[68] G.S. Chen, M. Okido, and T. Oki, Electrochemical studies of titanium in fluoride–chloride molten salts, *J. Appl. Electrochem.*, 18(1988), No. 1, p. 80.
[69] Y. Iwadate, T. Harada, T. Ohkubo, *et al*., Pulsed neutron diffraction study of $NaNO_2$ and $KNO_2$ pure melts, *Electrochemistry*, 77(2009), No. 8, p. 741.
[70] Y. Fang, C.H. Fang, L.J. Lin, and X.F. Qin, A study on the structure of calcium nitrate tetrahydrate molten salt, *Salt Lake Res.*, 2007, No. 1, p. 39.
[71] H.X. Zhou, F.Y. Zhu, W.C. Fang, Y.G. Zhou, H.Y. Liu, C.H. Fang, and Y. Fang, Effect of additives on phase transition temperature and undercooling temperature of $CaCl_2{\cdot}6H_2O$–$Ca(NO_3)_2{\cdot}4H_2O$ and their molten salt structure, *J. Mater. Sci. Eng.*, 37(2019), No. 1, p. 160.
[72] I.S. Perelygin and G.P. Mikhailov, Manifestations of ion-ion interaction in the Raman spectra of the nitrate ion, *J. Appl. Spectrosc.*, 48(1988), No. 5, p. 516.
[73] R.W. Berg, D.H. Kerridge, and P.H. Larsen, $NaNO_2$ + $NaNO_3$ phase diagram: New data from DSC and Raman spectroscopy, *J. Chem. Eng. Data*, 51(2006), No. 1, p. 34.
[74] K.C. Xu and Y. Chen, Temperature-dependent Raman spectra of mixed crystals of $NaNO_3$–$KNO_3$: Evidence for limited solid solutions, *J. Raman Spectrosc.*, 30(1999), No. 3, p. 173.
[75] S. Jayaraman, A.P. Thompson, O.A. von Lilienfeld, and E.J. Maginn, Molecular simulation of the thermal and transport properties of three alkali nitrate salts, *Ind. Eng. Chem. Res.*, 49(2010), No. 2, p. 559.
[76] N.A. Ponyatenko and I.V. Radchenko, Study of structure of binary fused monovalent nitratesd with $Ca(NO_3)_2$, $Ba(NO_3)_2$ and $Sr(NO_3)_2$ by the method of Raman scattering, *Ukr. J. Phys.*, 14(1969), No. 1, p. 20.
[77] N.A. Ponyatenko and I.V. Radchenko, Orientational interaction and rotational motion of the $NO_3^-$ ion in monovalent nitrate melts, *Opt. Spectrosc.*, 26(1969), p. 353.
[78] B.L. Gao, F.G. Liu, and Z.W. Wang, Raman spectra of $NaNO_2$–$KNO_3$–$NaNO_3$ ternary molten salts, *Rare Met.*, 28(2009), No. S1, p. 581.
[79] J.Y. Zhao, *Structure Study on the Ternary $NaNO_3$–$KNO_3$–$NaNO_2$ Molten Sallts* [Dissertation], Qinghai Normal University, Xining, 2020, p. 77.
[80] H.Y. Hou, J.L. You, Y.Q. Wu, H. Chen, and G.C. Jiang, Raman spectroscopic study of alkali carbonates, *Chin. J. Light. Scatt.*, 13(2001), No. 3, p. 162.
[81] L.J. Chen, J. Zuo, and C.J. Lin, *In-situ* Raman spectroscopy studies on the electrode process of cathode in MCFC, [in] *Proceedings of the 13th Chinese Symposium on Molecular Spectroscopy*, Xiamen, 2004, p. 199.
[82] H. Ohata, K. Takeuchi, K. Ui, and N. Koura, The structure of molten lithium carbonate calculated by DFT and MD simulations, *ECS Trans.*, 6(2007), No. 14, p. 57.
[83] N. Koura, S. Kohara, K. Takeuchi, *et al*., Alkali carbonates: Raman spectroscopy, *ab initio* calculations, and structure, *J. Mol. Struct.*, 382(1996), No. 3, p. 163.
[84] Y.Z. Wang, *Influence of Additives on the Structure and Properties of Aluminum Electrolysis Molten Salt system* [Dissertation], Kunming University of Science and Technology, Kunming, 2015, p. 93.
[85] S.L. Jiang, C.M. Ye, Y.L. Liu, *et al*., Insights into the effects of fluoride anions on the electrochemical behavior and solution structure of trivalent samarium in LiCl–KCl molten salt, *Electrochim. Acta*, 439(2023), art. No. 141733.
[86] J.L. You, T. Zhao, S. Petrik, Y.Y. Wang, and X.W. Liu, *In-situ* high temperature Raman spectroscopy and quantum chemical *Ab initio* simulation on species in molten NaF–$AlF_3$ fluorides, [in] *Proceedings of the 17th National Symposium on Molecular Spectroscopy*, Shaoguan, 2012, p. 223.
[87] J. Wang and C.L. Liu, Temperature and composition dependences of shear viscosities for molten alkali metal chloride binary systems by molecular dynamics simulation, *J. Mol. Liq.*, 273(2019), p. 447.
[88] Y.L. Liu, J.H. Lan, L. Wang, *et al*., The influence of $F^-$ ion on the electrochemical behavior and coordination properties of uranium in LiCl–KCl molten salt, *Electrochimica Acta*, 404(2022), art. No. 139573.
[89] Y.K. Wu, G.Q. Yan, S. Chen, and L.J. Wang, Electrochemistry of Hf(IV) in NaCl–KCl–NaF–$K_2HfF_6$ molten salts, *Int. J. Miner. Metall. Mater.*, 27(2020), No. 12, p. 1644.

[90] J.X. Song, Q.Y. Wang, J.Y. Wu, S.Q. Jiao, and H.M. Zhu, The influence of fluoride ions on the equilibrium between titanium ions and titanium metal in fused alkali chloride melts, *Faraday Discuss.*, 190(2016), p. 421.

[91] S.S. Liu, S.L. Li, C.H. Liu, J.L. He, and J.X. Song, Effect of fluoride ions on coordination structure of titanium in molten NaCl–KCl, *Int. J. Miner. Metall. Mater.*, 30(2023), No. 5, p. 868.

[92] R. Yuan, C. Lü, H.L. Wan, *et al*., Effect of fluoride addition on electrochemical behaviors of V(III) in molten LiCl−KCl, *Trans. Monferrous Met. Soc. China*, 32(2022), No. 8, p. 2736.

[93] X. Bai, S. Li, J. He, and J. Song, Effect of fluoride-ion on the electrochemical behavior of tantalum ion in NaCl–KCl molten salt, *J. Electrochem. Soc.*, 169(2022), No. 8, art. No. 082504.

[94] H. Guo, J. Li, H.L. Zhang, *et al*., Study on micro-structure and transport properties of KF–NaF–$AlF_3$–$Al_2O_3$ system by first-principles molecular dynamics simulation, *J. Fluorine Chem.*, 235(2020), art. No. 109546.

[95] C.Y. Wang, *Raman Spectroscopy and Theoretical Calculation of Metal Fluoride and Fluoride Oxides in Fluoride Molten Salt* [Dissertation], University of Chinese Academy of Sciences, Beijing, 2021, p. 135.

[96] X. Chen, H. Fu, and C. Wang, Influence of oxide ions on the speciation in molten KF–$ZrF_4$ and KF–$HfF_4$: A Raman spectroscopic and theoretical investigation, *J. Mol. Liq.*, 342(2021), art. No. 117476.

[97] X. Wang, C.F. Liao, and L.S. Luo, Effect of $Nd_2O_3$ on the properties and structure of $AlF_3$–(Na/Li)F–$Al_2O_3$ melt, *Chin. Rare Earth*, 38(2017), No. 5, p. 1.

[98] X.Y. Liu, Y.J. Li, B.Z. Wang, and C.Y. Wang, Raman and density functional theory studies of lutecium fluoride and oxyfluoride structures in molten FLiNaK, *Spectrochim. Acta A: Mol. Biomol. Spectrosc.*, 251(2021), art. No. 119435.